Modelling microwave scattering in the melting layer

C J Walden, G G Kuznetsov and A R Holt

Department of Mathematics, University of Essex, Wivenhoe Park, Colchester CO4 3SQ, UK

Abstract

A description is given of models developed for the electromagnetic scattering and absorption properties of melting hydrometeors. Particular attention is paid to the role of the internal structure, especially the topology, of these particles and how this evolves during the melting process. In common with previous treatments a simple spherical geometry is adopted, and the particles divided into one or two (core and shell) regions of uniform effective permittivity. In past work these effective permittivities have been derived via mixing formulae of the Maxwell-Garnett or Bruggeman type. Results obtained using such methods are compared with a new approach based on the coherent potential approximation familiar from the theory of composite materials. This incorporates a description of the scale of inhomogeneity within the particle, making it suitable for use at the higher frequencies relevant to TRMM radiometry. Our results suggest that the volume fraction and topology of the air component may play an important role in determining the electromagnetic properties. For particles with a size-dependent density characteristic of snowflakes suitable values of the parameters relating to the air content yield predicted reflectivity profiles for 13.8GHz as a function of height that agree favourably with those obtained from the TRMM precipitation radar. The selected parameter values are employed to investigate the behaviour at higher frequencies.

1. Introduction

In the context of retrieving profiles of rainfall rate from radiometric data, such as that provided by the TRMM Microwave Imager (TMI), it has become apparent that neglect of the radiative contributions of the melting layer in stratiform regions may introduce appreciable offsets in the retrieved values (Vivekanandan et al., 1990; Schols et al., 1999; Bauer et al., 2000). In particular, discrepancies may exist between the rainfall rates retrieved using TMI data alone and those derived from precipitation radar (PR) reflectivities. It has been suggested that these might be accounted for by incorporating the radiative effects of large melting aggregate snowflakes.

The motivation for the work described here was to implement a model for the scattering properties of mixed phase hydrometeors in the melting layer. Of central significance was the need to design a model that would remain applicable at the highest frequency (85.5GHz) employed by TRMM. In such circumstances the wavelength is small enough for the electromagnetic properties of the particles to become sensitive to their internal structure. One approach that has been proposed in this respect is the conjugate gradient fast Fourier transform (CGFFT) method (Meneghini and Liao, 2000). This is based on evaluation of the scattering properties of explicit realizations of melting particles, considered as assemblies of cubic cells. The work presented here takes a different approach, in which the particles are modelled as spherical bodies with an effective permittivity ε_{eff}. Although this strategy has been common in the past, our treatment differs in the method for determining ε_{eff}, and in the way the internal structure of the melting particles is modelled.

Traditionally mixing formulae such as those of Maxwell-Garnett (1904) and Bruggeman (1935) have been employed (Bohren, 1986; Klaassen, 1988; de Wolf et al., 1990; D'Amico et al., 1998). The derivation of these formulae may be understood by considering the polarization of inclusions in a self-consistently determined medium of permittivity ε_{eff}. The analysis relies on an assumption that the inclusions are small compared with the wavelength. In the present work we apply a technique borrowed from the theory of composite materials, viz. the coherent potential approximation (CPA) (Sheng, 1995). This accounts not only for the polarization of inclusions but also for the scattering from them. The latter becomes increasingly important as the wavelength is reduced.

The elements required in the modelling process may be categorised as follows:

(i) Macroscopic properties of the melting layer.

(ii) Properties of individual melting particles.

In order to provide estimates of quantities appropriate for incorporation into radiative transfer calculations one must consider two aspects in part (ii). Firstly one needs to model the structure of the particles and how this evolves during the melting process. Given this one must then go on to derive their electromagnetic properties. Within the present framework this involves derivation of an effective permittivity ε_{eff} followed by a standard application of scattering theory.

2. Macroscopic properties of the melting layer

The height of the upper boundary (the 0° C isotherm or freezing level) of the melting layer and its vertical extent depend on the vertical atmospheric temperature profile, which we may assume to be monotonic for relevant altitudes. The vertical extent is also strongly dependent on the size and mass density distributions of the initial unmelted hydrometeors. If we assume the temperature to be well approximated by a constant lapse rate of 6° C km^{-1}, the melting layer typically occupies a region 200 – 1000 m in height.

In order to model the reflectivity observed by the TRMM PR, and to facilitate estimation of radiometric quantities via radiative transfer calculations, it is important to model the scattering and absorption properties within a given atmospheric volume element. For frequencies of relevance to TRMM it is reasonable to assume an independent scattering approximation, for which the scattering properties of an individual hydrometeor do not depend on its proximity to other particles. In this regime scattering properties for a given volume element depend on the population of particles within that element, i.e. on the number density of particles of a given species with mass m, and mass fraction q of liquid water. Rather than work directly in terms of mass, it is convenient to label each particle according to the diameter D_{w} of raindrop it produces on complete melting. However, in doing so we neglect aggregation and break-up, so that each raindrop is assumed to have resulted from a single snowflake.

We now have for the coefficient of extinction in a volume element at position $\mathbf{r}$

$$\alpha_{\text{ext}}(\mathbf{r}) = \sum_{\text{species},s} \int_{q=0}^{1} \int_{D_{\text{w}}=0}^{D_{\max}} \sigma_{\text{ext}}(D_{\text{w}}, q, s) N(D_{\text{w}}, q, s, \mathbf{r}) dD_{\text{w}} dq \qquad (1)$$

where $\sigma_{ext}(D_w, q, s)$ denotes the extinction cross-section of a particle of species s with liquid water mass fraction q and melted diameter D_w, as appropriate. We may also define $\alpha_{sca}(\mathbf{r})$ by employing the scattering cross-section $\sigma_{sca}(D_w, q, s)$, and in a similar way find the reflectivity. The scattering albedo for this volume element is defined by

$$\omega = \frac{\alpha_{sca}(\mathbf{r})}{\alpha_{ext}(\mathbf{r})} \tag{2}$$

It is also useful to define the asymmetry parameter

$$g = \frac{1}{\alpha_{sca}(\mathbf{r})} \sum_{\text{species, } s} \int_{q=0}^{1} \int_{D_w}^{D_{max}} \overline{\mu}(D_w, q, s)\, \sigma_{sca}(D_w, q, s) N(D_w, q, s, \mathbf{r}) dD_w dq \tag{3}$$

where $\overline{\mu}(D_w, q, s)$ denotes the mean cosine of the scattering angle for a given particle.

Notice that we have introduced a maximum cut-off diameter D_{max} to reflect the mechanical instability of large raindrops. The quantity $N(D_w, q, s, \mathbf{r}) dD_w dq$ represents the number density of particles of species s with melted diameters in the interval from D_w to $D_w + dD_w$ and melted mass fraction between q and $q + dq$ in a volume element located at position $\mathbf{r}$. In general we may allow for a number of different particle species, e.g. graupel or aggregate snowflakes. However, in the present work we have assumed that the only distinction between particles is due to their mass m and their melted mass fraction q. Also, if we make an approximation in which the melting layer properties vary only in the vertical direction, we may directly link q with the altitude h of the particles. Hence, we may write

$$\alpha(h) = \int_{0}^{D_{max}} \sigma\left[D_w, q(D_w, h)\right] N\left[D_w, q(D_w, h)\right] dD_w \,. \tag{4}$$

The number density $N[D_w, q(D_w, h)]$ for particles in a volume element at altitude h may be derived from the drop-size distribution $N_w(D_w)$ for rain by applying mass conservation, so long as we ignore particle break-up and coalescence. For $N_w(D_w)$ we have employed a Marshall-Palmer distribution (Marshall and Palmer, 1948), although we have made a brief comparison with results obtained using a gamma distribution (Ulbrich, 1983).

Given the above assumption it follows that

$$N\left[D_w, q(D_w, h)\right] = \frac{V_w(D_w)}{V\left[D_w, q(D_w, h)\right]} N_w(D_w) \tag{5}$$

where $V[D_w, q(D_w, h)]$ is the terminal speed of a particle with melted mass fraction $q(D_w, h)$ and melted diameter D_w. $V_w(D_w)$ is the terminal speed of the resulting raindrop.

Following Wexler (1955) we assume for a given final diameter D_w that the product of fall speed and diameter remains constant, i.e.

$$V(D_w, q) D(D_w, q) = V_w(D_w) D_w \,. \tag{6}$$

Hence, provided with a model for how the diameter of a melting particle depends on its melted mass fraction q, together with a means for calculating $V_w(D_w)$, we may determine the fall speed $V(D_w,q)$.

In the work presented here we have employed the modified Gunn-Kinzer formula for $V_w(D_w)$ (see e.g. Brussaard and Watson (1995)). Fig. 1 shows the form of $V(D_w,q)$, for three values of D_w, employing a power law model for the snow mass density (see Section 3.1). Substitution with the formulae of Foote and du Toit (1969) appears to produce only minor differences to our final results.

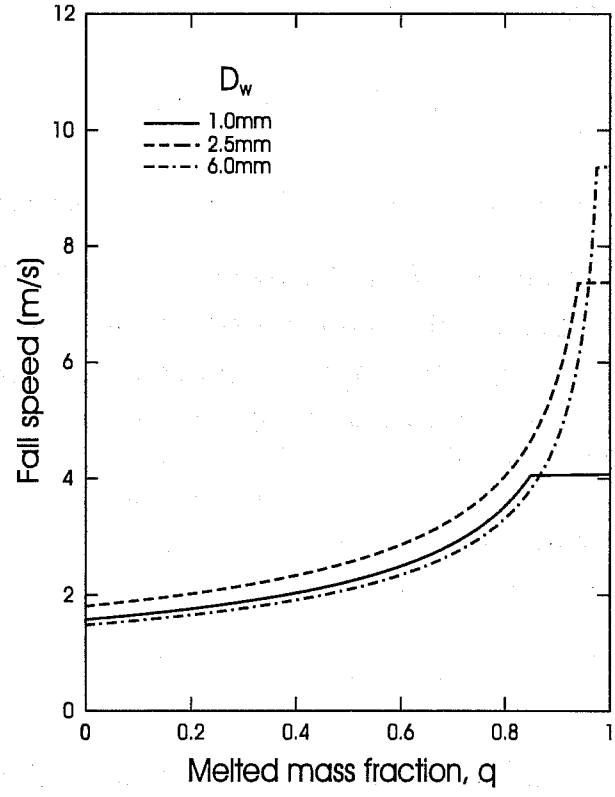

Fig. .1: Dependence of fall speed on melted mass fraction for a melting snowflake (with power law density – see Section 3.1). Three different masses are considered corresponding to different choices for the diameter D_w of the resulting raindrop.

In order to relate the cross-section and fall speed of a particle to its altitude h we need some way of determining the relationship between h and its melted mass fraction q. The following expression for the melting rate of a spherical snowflake was introduced by Wexler (1955)

$$L_f m \frac{dq}{dt} = 2\pi DF\left[k(T-T_0)+KL_v(\rho-\rho_0)\right] \tag{7}$$

where the following quantities are involved:

L_f, L_v latent heats of fusion and vaporization of water;

T, T_0 temperature of the surrounding air and the surface of the snowflake – we assume that $T_0 = 0^\circ$ C;

ρ, ρ_0 water vapour density in the air and near the surface of the snowflake;

k thermal conductivity of air;

K diffusivity of water vapour in air;

F ventilation factor – depends on the Reynolds number of the particle.

The left hand side of equation (7) represents the heat flux needed to melt a particle at a mass conversion rate $m(dq/dt)$. The right hand side describes the heat flux through the outer boundary of the particle and includes a description of heat loss due to evaporation. Combining equation (7) with the fall velocity allows us to predict the form of $q(D_w, h)$. Some typical results for snowflakes are shown in Fig. 2.

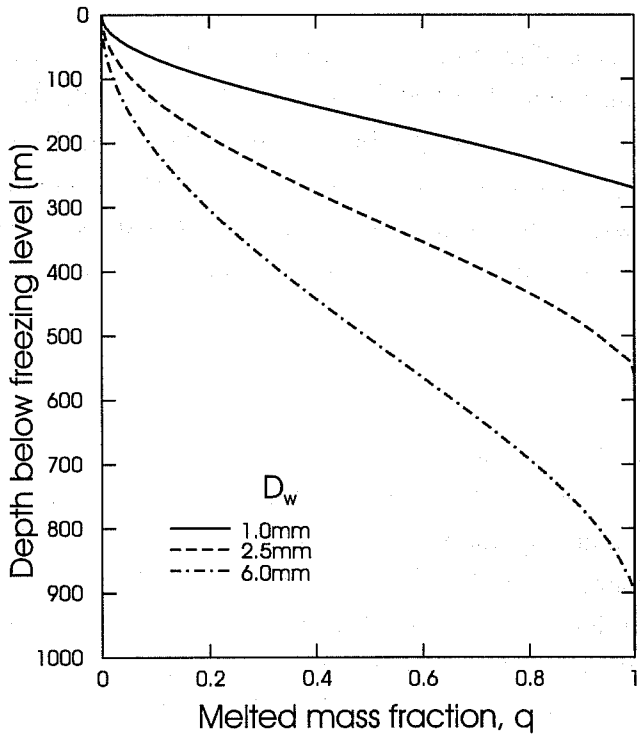

Fig. 2: Profile of melted mass fraction of snowflakes (with power law density – see Section 3.1) as a function of the distance fallen below the freezing level. Three different particle masses are considered corresponding to different raindrop diameters D_w.

However, this simple model does not take account of how heat is distributed inside the particle. Hence, we must make some assumptions with regard to how ice mass is redistributed as liquid water. We have developed a number of models for this. Section 3.3 gives a summary of their features, and the way in which results are influenced by the choice of model is described in Section 5.

3. Particle structure and thermodynamics

3.1 Snow mass density

Knowledge of the initial state of a dry particle is very important for simulating the melting process. Observations of precipitation have suggested that the density of a dry snowflake decreases with size (Magano and Nakamura, 1965; Locatelli and Hobbs, 1974; Mitchell et al., 1990), at least for large enough snowflakes. For other ice particles like graupel or hailstones the decrease in density with size is less marked.

The measured relationship between size (expressed in terms of an equivalent diameter, D_s) and mean mass density ρ_s can be fitted by the equation (Szyrmer and Zawadski, 1999)

$$\rho_s(D_s) = xD_s^{-y} \tag{8}$$

where x and y are constants. This is consistent with a mean density inside the particle that varies with distance r from its centre of mass via

$$\rho_{\text{interior}}(r) = \begin{cases} \dfrac{x(3-y)}{3} r^{-y} & \text{if } r_{\text{core}} < r < D_s/2 \\ \rho_{\text{core}} & \text{if } r \le r_{\text{core}} \end{cases}, \tag{9}$$

where we have introduced a core of radius r_{core} within which the density ρ_{core} is assumed to be uniform. This overcomes the problem of unphysical densities that would otherwise obtain for positive y. The value of r_{core} may be adjusted down to a minimum corresponding to a core density equal to that of pure ice ρ_{ice}. Notice that selecting $y = 0$ and $x = \rho_{\text{core}}$ we may also use equation (9) to describe particles whose mean density is uniform throughout their interior. Various suggestions for suitable values for the coefficients x and y have appeared in the literature. In this work we have used the empirical values of Mitchell et al. (1990), i.e. $x = 0.015\,\text{g cm}^{-2}$ and $y = 1$.

3.2 Melting modes

Given the above description, the question of specifying the sequence in which different zones of the particle melt has important consequences for the calculation of its diameter, fall speed and air content during the melting process. Suppose the density varies as in (9) and melting proceeds from the surface inwards. The rate at which the particle diameter shrinks will then be faster than if the ice melted everywhere inside at a rate proportional to the local ice mass density. This has led us to consider two descriptions of melting for any chosen model of the particle structure. The two principal categories are then subdivided into two further categories according to the way in which the air content of the particle is treated. Hence, we consider four melting modes in total.

3.2.1 Proportional melting

In this we assume that ice melts simultaneously in all regions of the particle and ignore the spatial distribution of ice. The snow (i.e. air and ice) volume is determined from

$$V_{\text{snow}} = \frac{(1-q)m}{\rho_s(D_s)} \tag{10}$$

where q is the melted mass fraction, m is the total mass, and $\rho_s(D_s)$ is the initial density of the unmelted particle [with initial diameter D_s given by equation (8)]. Note that $(1-q)m$ equates to the mass of the unmelted ice.

3.2.2 *Melting from the outside*

Here we assume that the particle melts from its outer edges, where the density of snow is smaller. In this case

$$V_{\text{snow}} = \frac{(1-q)m}{\rho_s(D_s')} \tag{11}$$

where D_s' is the equivalent diameter of the unmelted snow, and is defined by

$$(1-q)m = \rho_s(D_s')\frac{\pi D_s'^3}{6} \tag{12}$$

Note that this takes account of the fact that the mean density of the unmelted part increases as the particle melts.

3.2.3 *Displacement of air*

The amount of air contained within the melting particles turns out to have a strong influence on their electromagnetic properties. One reason for this is that the formation of air-water and air-wet ice interfaces tends to increase scattering processes within each particle, and this can lead to enhancement of the effective extinction cross-section. How one addresses the modelling of air expulsion during melting has important implications for the predicted attenuation. The issue rests on whether or not we allow water to displace air from the interior of the particle. We may consider two descriptions:

- The water remains separate from dry snow.
- The snow becomes wet by drawing water into the interior to fill the gaps between ice crystals in the snowflake skeleton. The air content of the particle is reduced as a consequence.

The effects of these on the particle composition and diameter are illustrated in Figs. 3 and 4. To help clarify Fig. 4 it is worth noting that the apex of the triangular plot corresponds to a fully melted particle with a water volume fraction of unity. The two lower corners refer to pure ice and pure air respectively. Points along any edge correspond to two-component mixtures, while interior points refer to three-component mixtures. The arrowed curves are trajectories in this composition space that are traced out as the particle melts.

One important feature to note from this plot is how much of the particle volume is taken up by air even after 50% of the ice mass has melted. This serves to reflect the tenuous nature of such aggregate snowflakes, as well as highlighting that melting modes 0 and 1 are not wholly appropriate for such particles. Despite this the expulsion of air by meltwater does not appear to have been considered in any previous treatment.

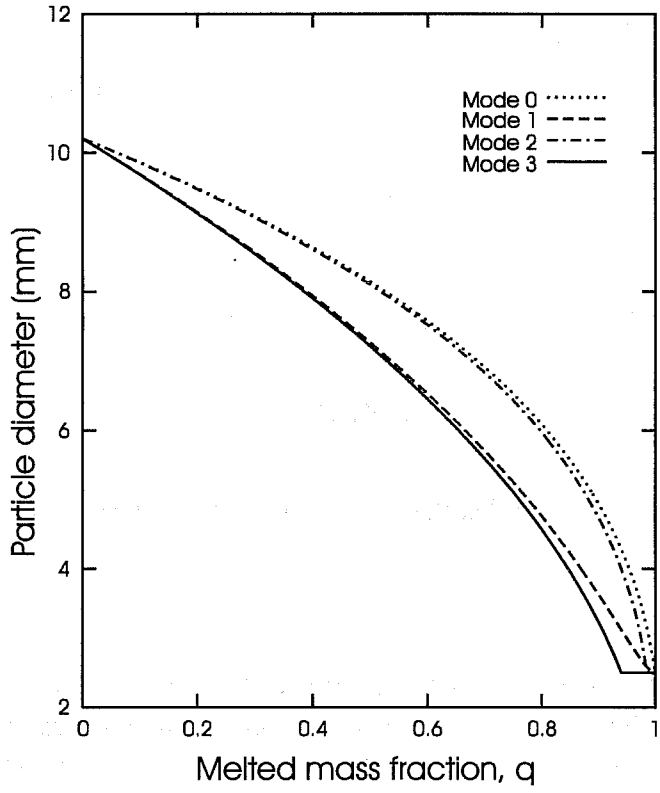

Fig. 3 Diameter of melting snowflake with D_w=2.5mm as a function of melted mass fraction for the four modes of melting. Modes 1 and 3 involve melting from the surface, whereas modes 0 and 2 involve conversion of ice to water throughout the particle. Modes 2 and 3 additionally involve the expulsion of air by the meltwater.

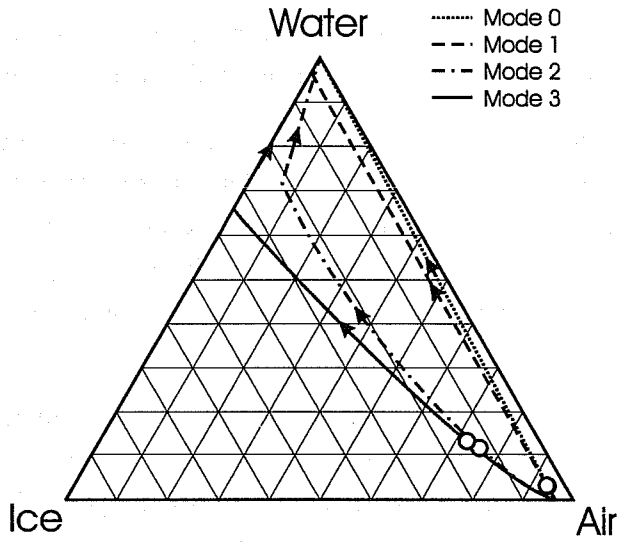

Fig 4 Ternary plot of evolution in the ice, air and liquid water volume fractions of a 2.5 mm particle during the melting process. The arrows indicate the direction in which the melted mass fraction q increases, and the open circles correspond to q=*0.5.*

For the majority of the results presented in Section 5 we have employed melting mode 3, on the basis that it appears to be more physically relevant for aggregate snowflakes. Modes for which the air is not expelled are more appropriate for denser particles such as hail or graupel. Since these latter particles are generally associated with convective processes we have not considered them in any great detail. However, it is worth

noting that cloud models generate populations of such particles within their simulation runs, so that there is some interest in predicting their electromagnetic properties.

3.3 Model descriptions

Any model of melting hydrometeors must make some assumptions concerning the structure of the particles. Prior studies of radar bright-band phenomena associated with the melting layer (D'Amico et al., 1998) have established that the density of the particles plays an important role in determining the strength of the scattering enhancement observed. We give below a brief description of each of the models we have considered.

In determining the required cross-section for each of these, it is necessary to replace the inhomogeneous mixture of air, ice and water by a uniform material with a representative dielectric constant. Some further details of how this is achieved will be provided in the next section. For all the models studied we have assumed a spherical symmetry. This was partly dictated by a desire to ensure the scattering calculations were tractable, and partly due to a lack of detailed knowledge on the shape of snowflakes.

3.3.1 Isotropic uniform and isotropic power law models

These are the simplest but also most flexible models we have considered. In the uniform case the snow mass density is homogeneous and fixed for all particles, whereas in the power law case it is given by equations (8) and (9). Although from the point of view of mass balance the power law model takes proper account of the non-uniformity of the internal snow density we have not attempted to incorporate this when calculating the scattering. Instead we treat the particle as a uniform spherical object with water randomly distributed inside.

3.3.2 Water shell model

This has been studied extensively in the past (Hardaker et al., 1995). It best describes dense particles such as hailstones. Melting proceeds from the surface inwards with the meltwater remaining outermost, forming a concentric shell around a dry snow core of constant mass density. For the purpose of calculating the electromagnetic properties we consider the object as a coated dielectric sphere, for which standard methods exist (Bohren and Huffman, 1983).

3.3.3 Isotropic dry core model

This is characterised by having the meltwater in the outer region of the particle. The particle melts from the surface inwards with the meltwater displacing air in an outermost shell. In other words, the outer region is a mixture of water and ice, and the inner region consists of ice and air. Once the water has displaced all air from the interior the particle further melting leads to the formation of a water shell around a water and ice core. Finally the ice skeleton disappears and particle becomes a water droplet. This model is designed to model particles with uniform ice mass density such as graupel.

3.3.4 Isotropic wet core model

This might be thought of as the complement to the isotropic dry core model. The assumption is that water is drawn into the body of the particle. This situation is quite possible for low density particles, especially those with a density that decreases towards the periphery. When the surface of the skeleton melts, the droplets of water that form at the outermost tips are drawn by capillary action into the body of the snowflake. The final

stages of melting resemble those of the dry core model in that a water shell forms around the outside. This model is designed for modelling a low-density aggregate snowflake, with the snow mass density described by (9).

3.3.5 Isotropic two-layer particle

This model is a variation of the wet core particle and is again designed for particles whose density varies as in (9). The idea that water droplets move inside the particle by capillary action can be extended by the assumption that water droplets can be trapped inside the particle by snow crystals when the density of ice is sufficiently large. For simplicity all particles above a certain size are assumed to have a core of the same fixed diameter. Water droplets are assumed to be randomly distributed inside this core, the aim being to mimic trapping at the joints of the ice skeleton (Fujiyoshi, 1986). When water fills all the volume of the core, the size of the core starts to grow according to the volume of the water. When all air has been displaced the particle acquires a water shell. Further details of this model may be found in a recent paper (Walden et al., 2000).

4. Electromagnetic properties of melting particles

4.1 Extinction, scattering and absorption cross-sections

Once a description for the structure of melting particles has been adopted we face the task of determining their scattering and absorption properties. For all cases described in Section 3.3 this process is simplified by the spherical symmetry. The main issue that remains concerns the treatment of the inhomogeneous interior of the particles. In common with previous approaches the inhomogeneous core and shell (if present) are replaced by regions of uniform effective permittivity.

In implementing this we have focused particularly on the topology of these regions, and how this evolves during the melting process. This can have a strong influence on the effective permittivity in a given region. Determining the extinction, scattering or absorption cross-section is then a simple matter of applying standard methods (Bohren and Huffman, 1983). An extension to a non-spherical geometry would be possible, although we have not explored it. It is perhaps worth noting that although spherical symmetry has been adopted with regard to the particle shape, this need not be imposed on its interior. For example D'Amico et al. (1998) have considered the case of aligned inclusions in order to model polarisation dependent properties.

4.2 Mixing formulae for the effective permittivity

As described above the melting of a snowflake produces mixed phase regions containing air, ice and water. For each of these we need to derive a representative picture by determining an effective permittivity ε_{eff}. A simple weighted average of the permittivities of the individual component materials is known to produce a poor representation of the true behaviour. This has led to the development of various mixing formulae, which attempt to capture the polarisability of the inhomogeneous medium. Central here are the formulae of Maxwell-Garnett (1904) and Bruggeman (1935), originally developed for two-component mixtures:

where ε_1 and ε_2 denote the permittivities of the individual components, and η is the volume fraction component 2. Which of these formulae applies depends on the topology. The Maxwell-Garnett formula is appropriate for a dispersion topology, where component 1 takes the form of inclusions in a matrix of component 2. The Bruggeman formula applies for a symmetric topology, in which neither component is identifiable as a host matrix. A schematic representation of these two topologies is shown in Fig. 5

When considering the permittivity of a mixture of more than two components the set of possible topologies is larger. It is not practical to account for all of these when deriving an effective permittivity, and instead we attempt to capture the essential features. For melting hydrometeors, which comprise a mixture of air, ice and water there have been a number of strategies proposed. Most of these involve breaking the calculation into two stages. Existing schemes include the following:

Bohren-Battan formula (Bohren and Battan, 1982) – 2-stage Maxwell-Garnett. ε_{eff} is calculated for inclusions of effective permittivity ε_{ia} in a water matrix. ε_{ia} is determined using the Maxwell-Garnett formula for ice inclusions in an air matrix.

Klaassen formula (Klaassen, 1988) – 2-stage Maxwell-Garnett. ε_{eff} is found for air inclusions in a medium of effective permittivity ε_{iw}, which itself is found via the Maxwell-Garnett formula for ice inclusions in a water matrix.

Modified Klaassen formula (Fabry and Szyrmer, 1999) – 2-stage Maxwell-Garnett. This is akin to the Bohren-Battan theory, but with inclusions of permittivity ε_{iw} in an air matrix. ε_{iw} is found by considering ice inclusions in a water matrix.

These are among the models evaluated by Fabry and Szyrmer (1999). However, unlike them we have considered only spherical inclusions in the present work. This is primarily to facilitate extension to the higher frequency regime via the CPA. Development of the latter to consider ellipsoidal inclusions is possible in principle, but has not been explored here.

In addition we may consider:

Symmetric formula for a three component mixture. This is a straightforward extension of the Bruggeman theory. All components are regarded as percolating the material. By this we mean that no one component can be viewed as either host or inclusion.

Non-symmetric formula for inclusions of one, two or three components in a single component host – extension of the Maxwell-Garnett theory.

Clearly, of the above five descriptions no individual one can truly represent the three-component mixture throughout the entire melting process. However, each formula will typically find application during some intermediate stage of melting. For example, the modified Klaassen formula is appropriate early in the melting process, but cannot be used in the last stage of melting where water is definitely the matrix. Since the effects one observes will represent an average over an ensemble of snowflake configurations, it seems reasonable to model the evolution in topology in this average sense, and avoid an abrupt switch between mixing formulae.

To achieve this we need to allow each component to appear both as inclusions and as part of a symmetric background. The proportion (by volume) of a given component that is allocated to inclusions is then allowed to vary depending on the volume fraction of that component. This reflects the fact that there will typically be a percolation threshold in volume fraction, below which the component exists only in the form of inclusions. The location of this threshold will depend on the typical length scale of inhomogeneity within the particle.

To implement this idea we have associated with each component material what we term a profile function. This provides a means for specifying the inclusion fraction of a given component, and allows us to model how the component evolves from inclusions to background matrix as its total volume fraction in the mixture increases. We determine ε_{eff} using the non-symmetric formula, viewing the mixed phase regions in a melting snowflake as composed of inclusions of the air, ice and water in a background matrix of effective permittivity $\varepsilon_{\text{symm}}$. This latter permittivity is calculated via the symmetric formula, on the assumption that the background is in fact a three-component mixture with a symmetric topology.

Although there is some flexibility in choosing the profile function, we have considered only functions with the simple ramp form depicted in Fig. 5 with different choices of η_1 and η_2. Provision for more complicated functions such as might be retrieved from experimental studies has been made within both the formalism and associated software. In the next section we compare results obtained for ramp profile functions with those from other mixing formulae.

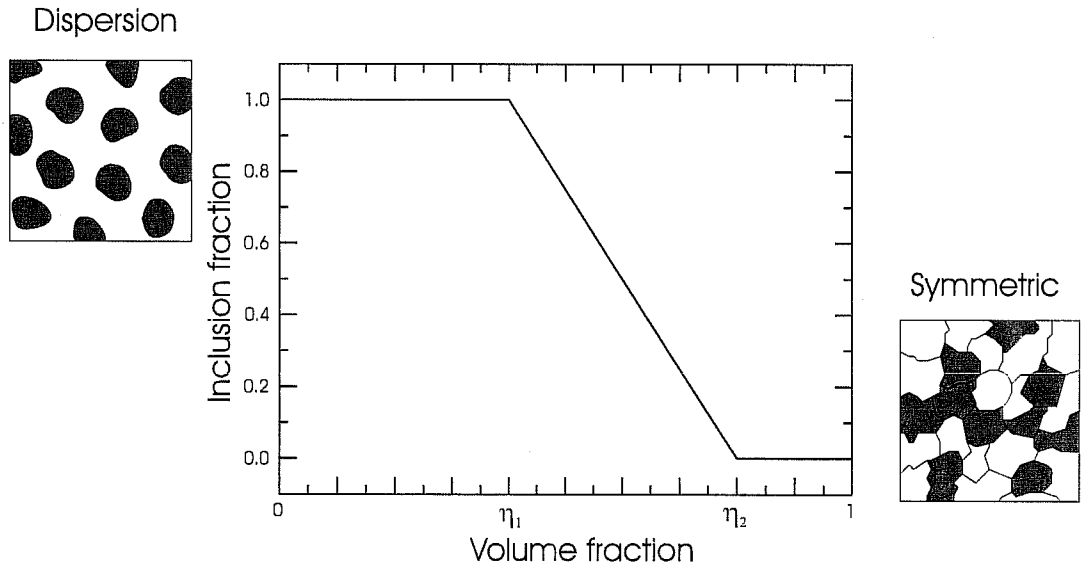

Fig. 5: Simple ramp permitivity profile function for interpolating between dispersion and symmetric topology. This function specifies the inclusion fraction of a given component as a function of its overall volume fraction. The insets provide a schematic representation of the two topologies.

4.3 The coherent potential approximation

The methods described above for calculating the effective permittivity make an inherent assumption that the local field is uniform on the scale of the inhomogeneity. This renders them valid for wavelengths long compared with the granularity of the media. However, as the wavelength is reduced scattering from the inhomogeneities becomes important. Attempts to account for this have led to the development of effective medium theories (Sheng, 1995) based on the coherent potential approximation (CPA) developed by Soven

(1967) for determining the electronic properties of disordered alloys. There appears to have been little attempt to apply these ideas to melting hydrometeors. A notable exception is due to Chýlek et al. (1991) who made contact with the CPA-based dynamic effective medium approximation of Stroud and Pan (1978).

To summarise the principles on which CPA theories are based, let us consider a two-component composite, which, as we have noted before, may exist in two distinct topological configurations. For each of these we select "structural units" as shown in Fig. 6.

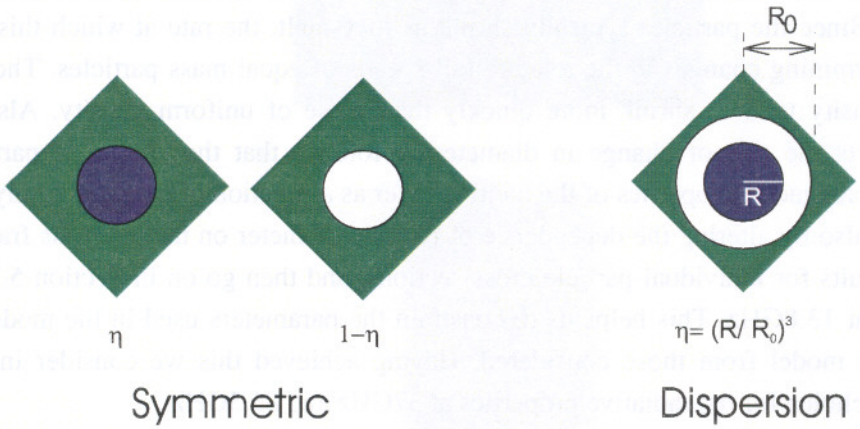

Fig. 6: Schematic representation of the structural scattering units employed in the CPA methods. Here, blue and white represent the individual components of the mixture, while green denotes the effective medium. η is the volume fraction of the blue component.

For the symmetric case we select inclusions with a size characteristic of the length scale of the microstructure, and imagine them to be embedded in an as yet undetermined effective medium. In the standard CPA the effective medium is determined from the following self-consistency argument. Consider a wave propagating through the effective medium. If that medium is to provide a faithful description of the average properties of the composite, then the following should be satisfied:

$$\eta f_1(0) + (1-\eta) f_2(0) = 0. \tag{14}$$

Here $f_1(0)$ and $f_2(0)$ are the forward scattering amplitudes associated with the inclusions of components 1 and 2 respectively, while η and $1-\eta$ are their corresponding volume fractions. We may interpret this as requiring that the introduction of inclusions in the otherwise uniform effective medium should produce no additional scattering on the average. It may be verified (Sheng, 1995) that this theory reduces to the Bruggeman result in the long-wavelength limit.

A similar equation obtains for the dispersion topology:

$$F(0) = 0\,, \tag{15}$$

where $F(0)$ now describes the scattering from a coated spherical inclusion (see Fig. 6) with the coating thickness chosen by considering the volume fraction of the dispersed component. The coated CPA reduces to the Maxwell-Garnett theory at long wavelengths.

In order to apply CPA-based methods in the present context it was necessary to generalise them to model three-component mixtures. Some further details of this are given in a recent paper (Walden et al., 2000). All the methods described in Section 4.2 have CPA analogues.

5. Results

Recall from Section 1 that the quantities of interest to radiative transfer modelling depend on both the cross-sections of the particles and their local number density. The latter is affected by the relative fall speeds of different particles. Since the particles typically shrink as they melt, the rate at which this happens clearly plays a role in determining changes in the relative fall speeds of equal mass particles. Those with a power law snow mass density tend to shrink more quickly than those of uniform density. Also, the choice of melting mode affects the rate of change in diameter. It follows that the choice of particle model may influence the electromagnetic properties of the melting layer as a function of height not only by affecting the cross-sections, but also by altering the dependence of particle diameter on melted mass fraction. In Section 5.1 we describe results for individual particle cross-sections, and then go on in Section 5.2 to consider the reflectivity profile at 13.8GHz. This helps us to constrain the parameters used in the modelling procedure, i.e. to select a best model from those considered. Having achieved this we consider in Section 5.3 the implications of our choice for the radiative properties at 37GHz and 85.5GHz.

5.1 Single particle properties

The scattering and absorption properties of a particle are strongly influenced by its composition and its geometry. To illustrate this consider Fig. 7, which shows results obtained for isotropic uniform and isotropic power law particles with melted diameter D_w = 2.5mm at 13.8GHz. The albedo shown here is the single-particle albedo $\omega_0 = \sigma_{sca} / \sigma_{ext}$, and the asymmetry parameter here equates to the mean cosine $\overline{\mu}$ of the scattering angle for this particle.

In all cases we have assumed the melting to take place from the surface, with the liquid water displacing the air in the interior. By using different methods to calculate the permittivity of the composite media, we obtain very different results for a particle with the same total mass and the same snow mass density.

In attempting to decide which of these might be most appropriate it is helpful to consider the way in which they treat air. For neither the Bohren-Battan nor Klaassen models is air allowed to percolate throughout the particle, being present only in inclusions. This does not seem to capture the likely behaviour in the early stages of melting. On the other hand the modified Klaassen model, in which air is always treated as the host matrix, does not seem reasonable either. Most promising would appear to be those methods that fall somewhere between by allowing the host matrix to evolve and change composition as the meltwater fraction increases.

These are based on use of a profile function such as the ramp function of Fig. 5. For ice the chosen values of η_1 and η_2 are 0.2 and 0.8 respectively. For air we select a different profile function. The results labelled Ramp0.8 correspond to $\eta_1 = 0.8$ with a fixed value of $\eta_2 = 1$. Water is always taken as part of the host rather than as inclusions. The argument for this is that water tends to wet the ice skeleton and therefore percolates throughout the particle. However, we have not made a systematic investigation of the effects of different water topologies.

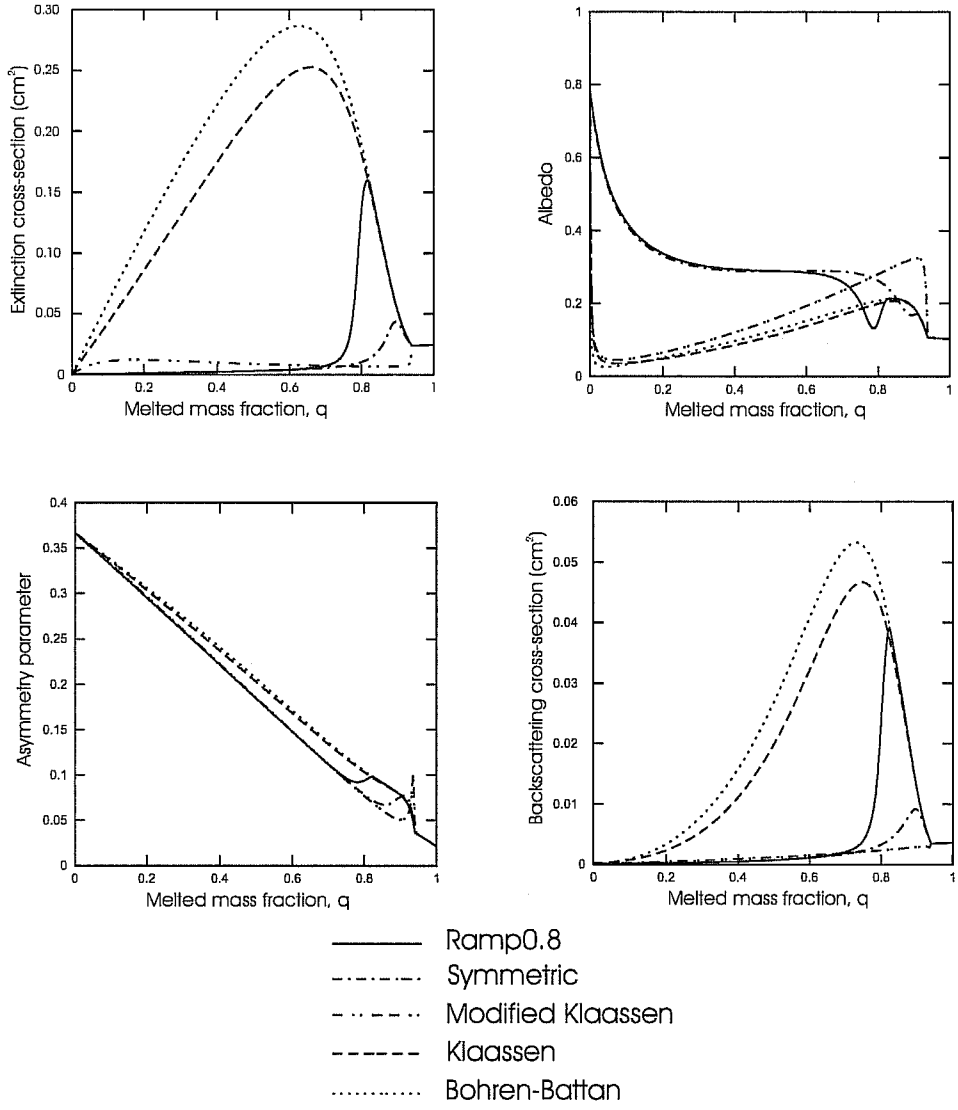

Fig. 7: Dependence of the extinction cross-section, single-particle albedo, asymmetry parameter and backscattering cross-section at 13.8GHz on the method of effective permittivity calculation. Results are given for a particle with melted diameter $D_w = 2.5\text{mm}$ *and a power law snow density with* $x = 0.015\text{gcm}^{-2}$ *and* $y = 1$ *[see equation (9)]. The different permittivity models are described in the text.*

Fig. 8 illustrates how the choice of particle geometry and in particular the distribution of meltwater can affect the electromagnetic properties during melting. We have not considered the dry core and water shell models for the case of a power law snow density since the outer regions are not dense enough to support a wet shell. Similarly, the wet core model is inappropriate for a dense particle. In all cases where a three-component mixture obtains we have employed the Ramp0.8 permittivity model.

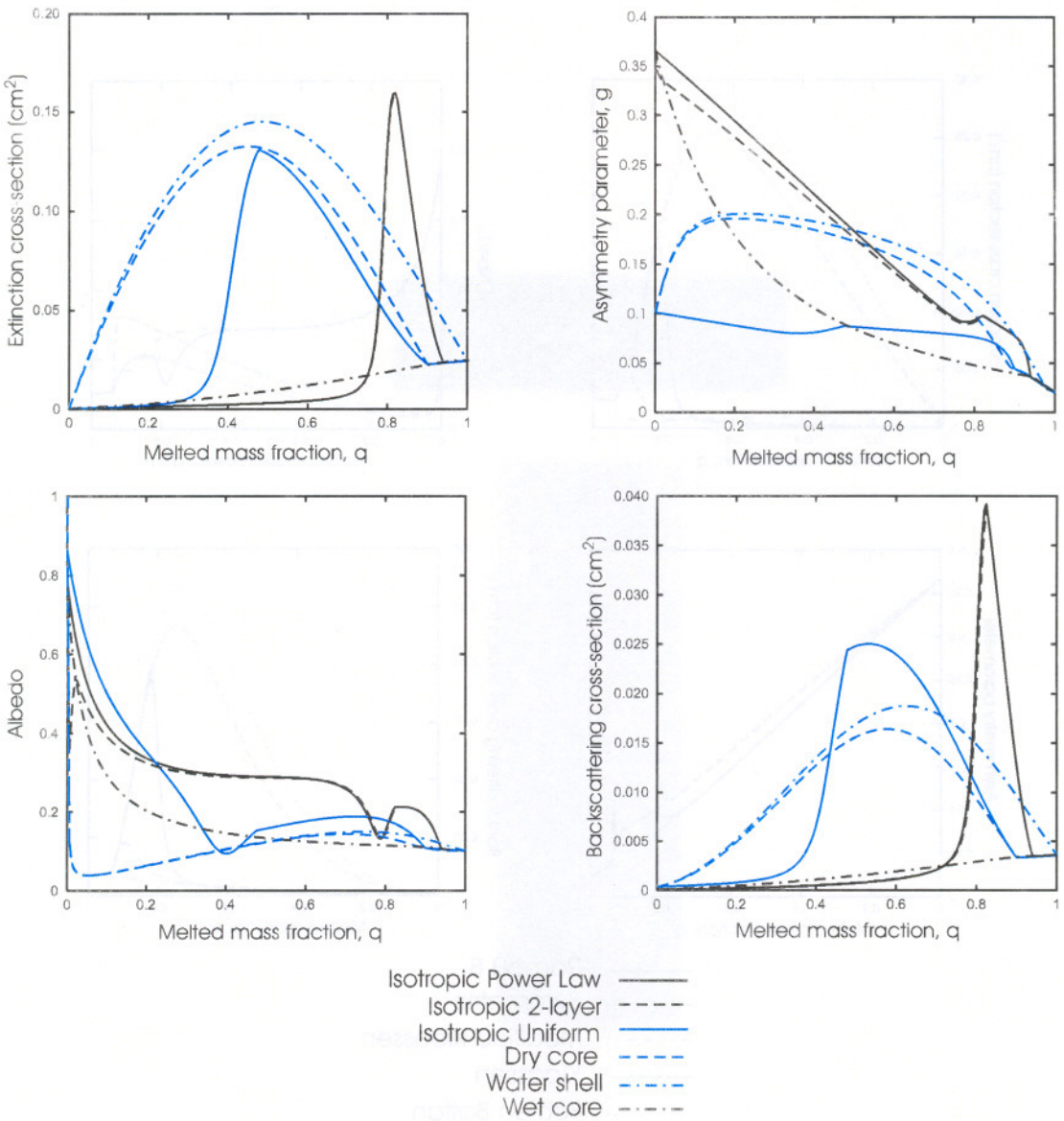

Fig. 8: Dependence of the extinction cross-section, albedo, asymmetry parameter, and backscattering cross-section on model choice as a function of melted mass fraction for particles with $D_w = 2.5\text{mm}$. *For isotropic power law and 2-layer models as well as the wet-core model the snow density is described by equation (9) with* $x = 0.015\text{gcm}^{-2}$ *and* $y = 1$. *The isotropic uniform, dry core and water shell models correspond to a snow density of* $\rho_s = 0.1\text{gcm}^{-3}$.

Although the above graphs help us gain some insight, it should be remembered that they are illustrative only of the behaviour for a fixed mass of particle. It is only after considering the behaviour for different masses that we can draw conclusions concerning the overall effects on the melting layer.

5.2 Reflectivity profile at 13.8GHz

Given the wealth of particle models and methods for determining the effective permittivity there is a clear need to reduce the parameter space by comparison with experimental data. To this end we have compared our predictions for the reflectivity as a function of height at 13.8GHz with average profiles obtained from

the TRMM PR. The idea is to gain some impression of how key features of the reflectivity profile are influenced by the parameters of the model.

The reflectivity in the rain region is fixed by the drop size distribution for a given rain rate. Once this is determined we are interested in how the reflectivity peak in the melting layer (i.e. the bright band) may be adjusted. D'Amico et al. (1998) have shown that this is strongly influenced by the mass density of the unmelted particles entering at the top of the melting layer. Lower density particles tend to provide greater enhancement of reflectivity. In their study they employed particles of uniform snow mass density. However, given that there are good arguments (Mitchell et al., 1990) favouring the power law density of equation (9), it seems desirable not to consider the snow density as a free parameter. Instead we have retained the model of equation (9) and varied instead the way in which the ice, water and air components are treated. In particular we have found that varying the topology of the air component can have a marked effect on the reflectivity profile. Specifically we have employed melting mode 3, so that the air is displaced by liquid water, and varied the permittivity profile function (See Fig. 5) for the air component. The permittivity profiles for the ice and water components are held fixed. Fig. 9 illustrates our findings.

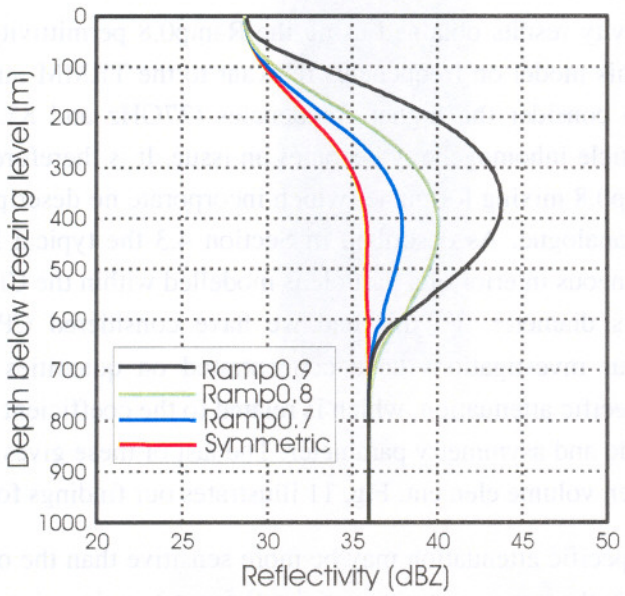

Fig. 9: Dependence of the reflectivity profiles at 13.8GHz on the topology of the air component. Results are shown for particles with a power law snow density as in equation (9) with $x = 0.015\text{gcm}^{-2}$ *and* $y = 1$, *and for a rainrate of 5.1mm/h. Three permittivity profiles are considered for air. Ramp0.7 denotes a profile function of the ramp form (Fig. 5) with* $\eta_1 = 0.7$ *and* $\eta_2 = 1.0$. *Ramp0.8 and Ramp0.9 refer to similar profile functions in an obvious notation. In each case the topology of the ice component is modelled using a ramp function with* $\eta_1 = 0.2$ *and* $\eta_2 = 0.8$, *whilst liquid water is always treated as host rather than inclusions. Comparison is given with the case where the air is always in the symmetric topology.*

Fig. 10 provides a comparison of the Ramp0.8 case with results obtained from the TRMM PR, showing good agreement at both 3.8 mm/h and 5.1 mm/h.

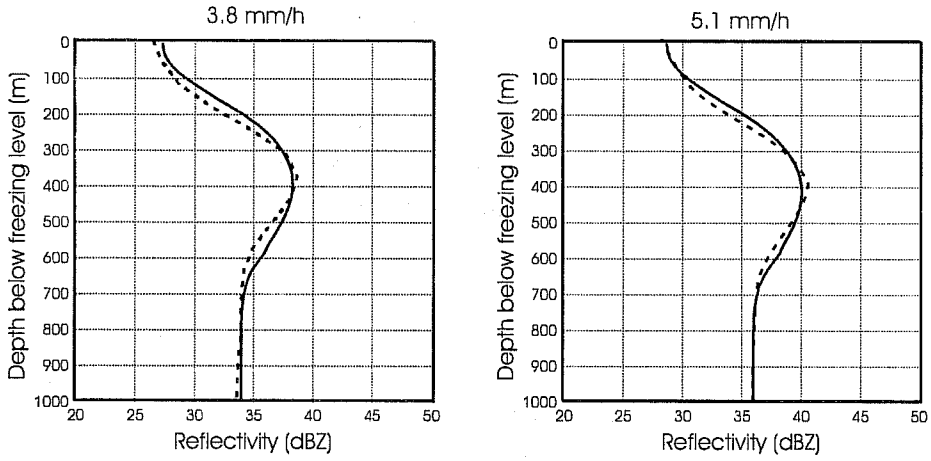

Fig. 10: Reflectivity profiles for the Ramp0.8 permittivity model at two different rainfall rates (solid curves) compared with profiles obtained from the TRMM PR (dashed).

5.3 Higher frequencies and the effects of granularity

Given the favourable reflectivity results obtained using the Ramp0.8 permittivity model it is of interest to explore the implications of this model on frequencies relevant to the TRMM microwave imager (TMI). In particular it is instructive to consider the higher frequencies (37GHz and 85.5GHz) as the question of sensitivity to the scale of particle inhomogeneity becomes an issue. It is therefore important to compare the results derived from the Ramp0.8 mixing formulae (which incorporate no description of length scales) with those obtained from a CPA analogue. As described in Section 4.3 the typical length scale or granularity associated with the inhomogeneous interior of a particle is modelled within the CPA by employing structural units (i.e. inclusions) of this diameter. To this end we have considered CPA inclusions of diameter $d = 0.2\text{mm}$ and 0.5mm. Our investigations have concentrated on quantities of relevance to radiative transfer. These include the specific attenuation, which is related to the coefficient of extinction by a constant factor, together with the albedo and asymmetry parameter. The last of these gives a measure of the degree of forward scattering from a given volume element. Fig. 11 illustrates our findings for a rainfall rate of 5mm/h.

Our results suggest that the specific attenuation may be more sensitive than the other quantities to the grain structure of the particle, with the coarser structure ($d = 0.5\text{mm}$) giving rise to a greater enhancement within the melting layer. The effect is particularly noticeable at 85.5GHz where the peak value is more than 10% higher than that derived from the mixing formula. Inspecting the albedo at this frequency we see that a significant part of the above increase is attributable to an enhancement of the absorption. This is not repeated at 37GHz and is perhaps a reflection that the inclusions do not represent such strong scatterers at lower frequencies, and therefore their size has less of an impact on the effective permittivity ε_{eff}. For neither frequency is the asymmetry parameter strongly influenced by the grain size. This is perhaps not surprising since it is generally expected to be most sensitive to the overall diameter of the hydrometeors with large particles causing more forward scattering. This is reflected in the graphs, where the large unmelted snowflakes at the freezing level scatter predominantly in the forward direction while the smaller raindrops cause more off-axis scattering. In attempting to interpret the behaviour at intermediate heights one must bear in mind that the local particle population will be modified according to equation (5). This tends to skew the

skew the distribution within the melting layer in favour of larger particles, which may help to account for the non-monotonic behaviour seen for 37GHz.

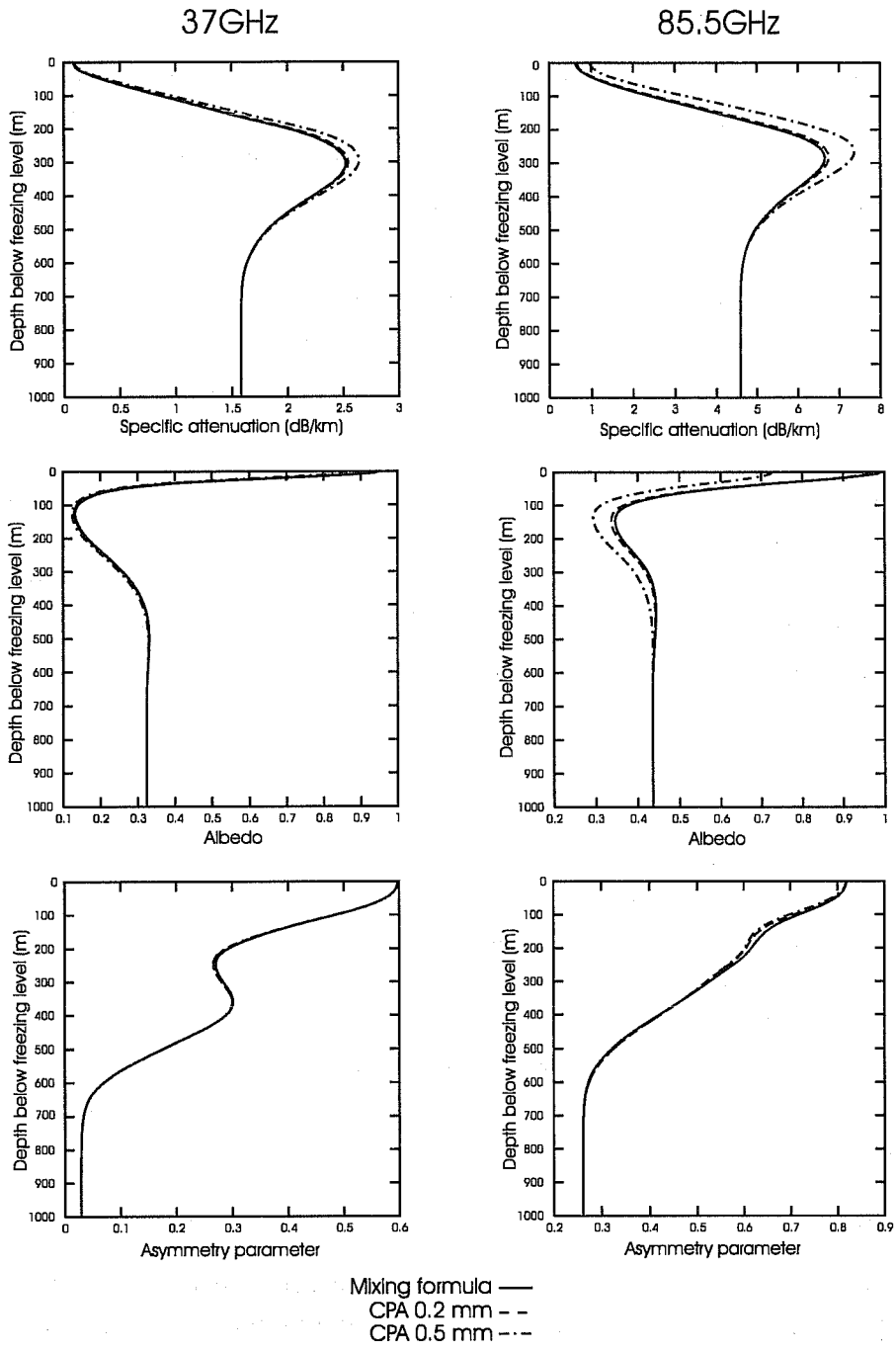

Fig. 11: Profiles as a function of depth below the freezing level of the specific attenuation, albedo and asymmetry parameter. Results are shown for the two highest TMI frequencies (37GHz and 85.5GHz), and comparison made between those derived from the Ramp0.8 mixing formula and CPA analogues of this with differing grain size (0.2mm and 0.5mm). In all cases an isotropic power law model (equation(9)) was adopted with with $x = 0.015\text{gcm}^{-2}$ *and* $y = 1$, *and a rainfall rate of 5mm/h.*

6. Discussion

It is clear from the preceding sections that the modelling of melting snowflakes involves a number of diverse considerations. In attempting to constrain the available parameter space one needs to draw on

arguments concerning physical suitability, numerical stability and tractability. The models described above are intended to strike a balance between providing an accurate description of the physics and producing a model that is computationally useful. It may be argued that certain features are more desirable than others. One that appears to have a central influence is the way in which the topology is described, especially that of the air component. Another is the mass density.

In our case we have chosen to retain the power law density of equation (9), since there appear to be strong independent arguments for this. However, given the aggregation processes by which such snowflakes are created, one might argue that our description fails to capture the fractal nature of such objects. In particular, we make no allowance for the size distribution of air pockets, which may influence the electromagnetic properties via the effective permittivity ε_{eff}. Looking at Fig. 11 it is clear that the length scale on which inhomogeneities occur can have important implications for the higher TMI frequencies. It would therefore be of interest to consider a hierarchical approach to determining ε_{eff} in which some account is taken of the different length scales present in the snowflake. To what extent this is feasible for a melting object remains to be seen.

What can be gleaned from our results is that the CPA (which is more appropriate for higher frequency calculations) together with our selected permittivity profile function provides an enhancement at 37GHz and 85.5GHz of the scattering and absorption over and above that predicted by standard methods. In particular, the increased absorption at 85.5GHz suggests that incorporating the model into radiative transfer calculations might account for the observed brightness temperatures. For 19.35GHz and 10.7GHz we found the influence of grain size to be less significant, so that the computationally simpler mixing formulae were adequate. This is true also for the reflectivity at 13.8GHz, which justifies our use of the mixing formulae in selecting the Ramp0.8 model.

In view of the fact that 13.8GHz PR data alone have been employed to constrain the parameters of our model any conclusions we draw must be regarded as subject to further validation. Nevertheless, it does appear from physical arguments that models which account for the evolution in topology of the mixed-phase particle are likely to produce the most reliable estimates. On this basis we tentatively propose the isotropic power law model with a Ramp 0.8 profile function as an appropriate model for microwave scattering by melting snowflakes. However, further constraints are needed to determine the optimal description of the grain structure within such objects, and for this purpose scattering measurements at frequencies in the 35-90GHz range would be of great assistance.

7. Conclusions

We have explored a number of models for the scattering of microwaves in the melting layer, and introduced a new approach based on the CPA. This is designed to take better account of the internal structure within the melting particles. Compared with previous methods we have focused on the change in topology of the hydrometeors that accompanies the melting process. In particular we have devised a means for modelling the interchange of air and water as host material, and shown how variation of the air topology allows us to constrain our model using 13.8GHz TRMM PR reflectivity profiles.

For higher frequencies the constrained model predicts enhancements in the scattering and absorption of microwaves that may account for what is observed in the retrieved TRMM brightness temperatures. Questions remain, however, with regard to the most appropriate length scale to employ within the CPA,

since the 85.5GHz results appear to be quite sensitive to this parameter. Further investigation will be necessary before firm conclusions can be drawn on this point.

In summary the topology-dependent parameterisation of melting snowflakes provides a description of the reflectivity profiles at 13.8GHz that agree well with measured values. The adoption of this parameterisation within CPA-based methods provides estimates for the specific attenuation, albedo and asymmetry parameter that may incorporated into radiative transfer calculations at TMI frequencies. The extent to which these agree with observations remains to be seen, but certainly demands an appropriate description of the scale of inhomogeneity within the hydrometeors.

Acknowledgements

The EuroTRMM program, funded by the European Commission and European Space Agency involves a consortium of scientists from Centre d'Etude des Environnements Terrestre et Planétaires (France), European Centre for Medium Range Weather Forecasting (UK), German Aerospace Research Establishment (Germany), Istituto di Fisica dell'Atmosfera (Italy), Max Planck Institute for Meteorology (Germany), Rutherford Appleton Laboratory (UK), University of Essex (UK), Université Catholique de Louvain (Belgium) and University of Munich (Germany).

References

D'Amico, M. M. G., A. R. Holt and C. Capsoni, 1998: An anisotropic model of the electromagnetic properties of the melting layer, *Radio Sci.*, **33**, 535-552.

Bauer, P., A. Khain, A. Pokrovsky, R. Meneghini, C. Kummerow, F. Marzano and J. P. V. Poiares Baptista, Combined cloud-microwave transfer modelling of stratiform rainfall, 2000, *J. Atmos. Sci.*, **57**, 1082-1104.

Bohren, C. F., 1986: Applicability of effective-medium theories to problems of scattering and absorption by nonhomogeneous atmospheric particles, *J. Atmos. Sci.*, **43**, 468-475.

Bohren, C. F. and L. J. Battan, 1982: Radar backscattering of microwaves by spongy ice spheres, *J. Atmos. Sci.*, **39**, 2623-2629.

Bohren, C. F. and D. R. Huffman, 1983: *Absorption and Scattering of Light by Small Particles*, Wiley, 530 pp.

Bringi, V. N., R. M. Rasmussen and J. Vivekanandan, 1986: Multiparameter radar measurements in Colorado convective storms. Part I: Graupel melting studies, *J. Atmos. Sci.*, **43**, 2545-2563.

Bruggeman, D. A. G., 1935: Berechnung verschiedener physikalischer Konstanten von hetarogenen Substanzen: I. Dielectrizitätskonstanten und Leitfahigkeiten der Mischkörper aus isotropen Substanzen, *Ann. Phys. Lpz.*, **24**, 636-679.

Brussaard G., and P. A. Watson, 1995: Atmospheric modelling and millimetre wave propagation, Chapman and Hall, London.

Chýlek, P., R. G. Pinnick and V. Srivastava, 1991: Effect of topology of water-ice mixtures on radar backscattering by hailstones, *J. Appl. Meteor.*, **30**, 954-959.

Fabry, F. and W. Szyrmer, 1999: Modelling of the melting layer. Part II Electromagnetic, *J. Atmos. Sci.*, **56**, 3593-3600.

Foote A. G. B., and P. S. du Toit, 1969: Terminal velocity of raindrops aloft, *J. Appl. Meteor.*, **8**, 249-253.

Fujiyoshi, Y., 1986: Melting snowflakes, *J. Atmos. Sci.*, **43**, 307-311.

Hardaker, P., A. R. Holt and C. G. Collier, 1995: A melting-layer model and its use in correcting for the bright band in single-polarization radar echoes, *Quart. J. Roy. Meteor. Soc.*, **121**, 495-525.

Klaassen, W., 1988: Radar observations and simulation of the melting layer of precipitation, *J. Atmos. Sci.*, **45**, 3741-3753.

Locatelli, J. D., and P. V. Hobbs, 1974: Fall speeds and masses of solid precipiation particles, *J. Geophys. Res.*, **79**, 2185-2197.

Magano, C., and T. Nakamura, 1965: Aerodynamic studies of falling precipitation particles, *J. Meteor. Soc. Japan*, **43**, 139-147.

Marshall, J. S., and W. M. K. Palmer, 1948: The distribution of raindrops with size, *J. Meteor.*, **5**, 165-166.

Maxwell-Garnett, J. C., 1904, Colours in metal glasses and in metallic films, *Phil. Trans. Roy. Soc. Lond.*, **203**, 385-420.

Meneghini, R., and L. Liao, 2000: Effective dielectric constants of mixed-phase hydrometeors, *J. Atmos. Oceanic Technol.* **17**, 628-640.

Mitchell, D. L., R. Zhang and R. L. Pitter, 1990: Mass-dimensional relationships for ice particles and the influence of riming on snowfall rates, *J. Appl. Meteor.*, **29**, 153-163.

Schols, J. L., G. D. Alexander, R. E. Stewart, I. J. Angus and A. C. L. Lee, 1999: Microwave properties of frozen precipitation around a North Atlantic cyclone, *J. Appl. Meteor.* **38**, 29-43.

Sheng, P., 1995: Introduction to Wave Scattering Localization, and Mesoscopic Phenomena, Academic Press, San Diego.

Soven, P., 1967: Coherent-potential model of substitutional disordered alloys, Phys. Rev. 156, 809-813.

Stroud, D., and F. P. Pan, 1978: Self-consistent approach to electromagnetic wave propagation in composite media: application to model granular materials, *Phys. Rev. B*, **17**, 1602-1610.

Szyrmer, W. and I. Zawadski, 1999: Modeling of the melting layer. Part I: Dynamics and microphysics, *J. Atmos. Sci.*, **56**, 3573-3592.

Ulbrich, C. W., 1983: Natural variations in the analytical form of the raindrop size distribution, J. Climate and Appl. Meteor., **22**, 1764-1775.

Vivekanandan, J., J. Turk, G. L. Stephens and V. N. Bringi, 1990: Microwave radiative transfer studies using combined radar and radiometer measurements during COHMEX, *J. Appl. Meteor.* **29**, 561-585.

Walden, C. J., G. G. Kuznetsov and A. R. Holt, 2000: Topology dependent modelling of microwave scattering from melting snowflakes, *Electronics Lett.*, **36**, 1494-1496.

Wexler, R., 1955: *The Melting Layer*, Vol. 3, *Meteorological Radar Studies*, Blue Hill Observatory, Harvard University, 29 pp.

de Wolf, D. A., H. W. J. Russchenberg and L. P. Ligthart, 1990: Effective permittivity of and scattering from wet snow and ice droplets at weather radar wavelengths, *IEEE Trans. Antennas Propag.* , **38**, 1317-1325.